International Journal of Humanoid Robotics
Vol. 15, No. 1 (2018) 1850015 (21 pages)

DOI: 10.1142/S0219843618500159

World Scientific
www.worldscientific.com

Active Tactile Exploration Based on Cost-Aware Information Gain Maximization

Simon Ottenhaus*, Lukas Kaul, Nikolaus Vahrenkamp and Tamim Asfour†

Institute for Anthropomatics and Robotics (IAR),
Karslruhe Institute of Technology (KIT),
Adenauerring 2, 76131 Karlsruhe, Germany
**simon.ottenhaus@kit.edu*
†*asfour@kit.edu*

Received 1 May 2017
Accepted 22 January 2018
Published 28 February 2018

Active tactile perception is a powerful mechanism to collect contact information by touching an unknown object with a robot finger in order to enable further interaction with the object or grasping of the object. The acquired object knowledge can be used to build object shape models based on such usually sparse tactile contact information. In this paper, we address the problem of object shape reconstruction from sparse tactile data gained from a robot finger that yields contact information and surface orientation at the contact points. To this end, we present an exploration algorithm which determines the next best touch target in order to maximize the estimated information gain and to minimize the expected costs of exploration actions. We introduce the *Information Gain Estimation Function* (*IGEF*), which combines different goals as measure for the quantification of the cost-aware information gain during exploration. The IGEF-based exploration strategy is validated in simulation using 48 publicly available object models and compared to state-of-the-art Gaussian processes-based exploration approaches. The results show the performance of the approach regarding exploration efficiency, cost-awareness and suitability for application in real tactile sensing scenarios.

Keywords: Tactile exploration; next best touch; object modeling; Gaussian processes.

1. Introduction and Related Work

As humanoid robots move from the laboratory to real-world environments, they need to be able to manipulate unknown objects. Among others, such manipulation tasks require an understanding of the geometric shape of such objects, which can be acquired through different sensor modalities. While camera-based vision might be the most obvious modality to use, it can be impaired by either the object

† Corresponding author.

properties (e.g., reflecting, translucent, uniformly colored) or the environmental conditions (e.g., poor lighting, fog, bright sunshine). To overcome these shortcomings, tactile sensing can be used to gather additional information, which also plays an important role in human grasping.[1] Recent research has demonstrated the close link between tactile object exploration and grasp planning based on tactile information.[2]

Other interesting applications of haptic sensing exist, such as object discrimination from multimodal haptic data,[3] detecting object affordances directly from tactile interaction[4,5] or object localization using a Bayesian approach.[6] However, in this paper, we focus on the aspect of geometric modeling.

To acquire object shape information through tactile exploration three problems must be solved: (1) how to collect contact information by efficiently selecting the next best touch on the object surface, (2) how to generate object shape models based on the acquired sparse tactile data, and (3) how to either control the robot hand or fingertips to make contact and follow trajectories between contacts or how to control sliding motions on the surface of the object.

An extensive body of work has been conducted in the literature to address these questions. The first two problems can be addressed simultaneously by employing dynamic potential fields for exploration.[7] For geometric modeling, superquadrics or decompositions of multiple superquadrics have been used to parametrically estimate the object surface.[8–10] Other approaches use geometric primitives to compose the explored object.[11,12] For object modeling based on vision data, estimating the back side of the object is of special interest and often performed by leveraging assumed object symmetries.[13–16] One popular choice for object modeling are *Gaussian Processes Implicit Surfaces* (*GPIS*),[17] that have recently been applied extensively to the field of haptic exploration.[18–22] Building on GPIS, an extension to incorporate prior knowledge has been proposed to enhance the probabilistic reconstruction of explored objects.[23]

The data acquisition by tactile sampling, that underlies object shape modeling approaches, requires a strategy for the generation and execution of exploratory actions. A human-inspired haptic exploration strategy has been proposed for acquiring tactile data with a multi-finger hand[24,25] and next-best-touch algorithm based on an information gain metric has been proposed and demonstrated on an ARM-S robot.[26] A different approach for classification of previously-known objects uses the classification boundary to guide the exploration toward more informative areas.[27] A data-driven object recognition procedure was proposed relying on an optimal action generator for planning of exploratory actions, subsequently extracting the object manifold using Gaussian Process Latent Variable Models (GPLVM).[28] Contact data for estimating environmental constraints of the robot workspace can be estimated from joint-level proprioceptive sensing.[29]

Other exploration approaches suggested to maximize the newly acquired information about the object by moving the robot hand to the region with highest model uncertainty.[19,22] This approach is based on Gaussian processes while using

the variance of the Gaussian process as a guiding function. A similar idea underlies another work with the notable difference that the tactile sensor is continuously guided along the surface without breaking contact.[30] While this method provides much denser contact information and leads to impressive results regarding surface reconstruction, the experimental setup is limited to mainly convex and smooth objects. In the case of discrete tactile sampling, using the Gaussian process variance (GP-V) for next best target selection during haptic exploration might not be the best approach, since the area with the highest variance is often far away from the current position of the robot hand. It is therefore advisable to consider the exploration cost in form of the distance traveled by the exploring robot finger in the exploration strategy. This idea has already been brought forward by Caselli *et al.* for the exploration of convex objects.[31] In their recent work, Matsubara *et al.* consider the travel cost during exploration of 3D objects, while the path planning and shape estimation problem is reduced to 2D space.[21] Tosi *et al.* also consider the exploration cost in form of execution time and its trade-off with uncertainty reduction in order to localize objects.[32] They elegantly summarize the problem of the optimal exploration strategy by asking the question "where to sense next?". While most of the work in this area is formulated for one single end-effector, a recent study has proposed an extended exploration algorithm that can leverage the data provided by a sensor-equipped multi-fingered hand.[33]

The work presented in this paper adopts and integrates several of the aforementioned key ideas: exploration is guided in a way that aims at maximizing the shape information gain, while simultaneously minimizing the travel cost in terms of traveled fingertip distance in between successive contact points. The information gain is estimated using several information heuristics, and the trajectory planning uses cubic Bézier curves, which are particularly well-suited for manipulator trajectory generation since they are easy to compute, provide continuous and smooth paths and allow parametrization of the approach direction.

The presented strategy is extensively evaluated on 48 objects from the publicly available YCB object and model set[34] and compared to the state-of-the-art approach based on the GP-V as a guiding function. We show that the proposed strategy outperforms the GP-V approach when considering four different metrics regarding exploration efficiency and suitability for application in real tactile sensing scenarios.

The paper is organized as follows. In Sec. 2, the new exploration algorithm and the selection of the next-best-touch target are introduced. Building on the Information Gain Estimation Function (IGEF) different exploration goals are combined to enable the cost-aware information gain during exploration. Section 3 presents an extensive evaluation of the developed approaches using 48 objects from the YCB object and model set. Section 4 concludes the paper and discusses future extensions and research directions.

2. Exploration Strategy

In order to explore an unknown object, the fingertip of the robot's hand has to touch the object. To initialize the exploration procedure, we assume that the first touch target is known, either manually given by the operator or extracted from visual information. Once the robot has reached the first contact point on the object, an initial surface can be estimated based on the acquired contact and the exploration process can be started.

The exploration procedure can be briefly summarized as follows: a point on the estimated surface is selected. An exploratory action is generated to move the fingertip to the touch target. The fingertip follows the generated trajectory until a contact is detected. The contact is added to the surface model and the next touch target is selected for exploration. The entire algorithm is described in Algorithm 1.

One way to accomplish such an exploratory step is to retract the hand completely and approach the object again to move to the touch target position. This can be an effective way to minimize the risk of unwanted collisions with the object. One drawback is that the complete retraction and approach of the hand takes time during exploration. An alternative way is to plan a continuous, smooth trajectory from the current position of the fingertip to the next best touch target. The goal is to minimize the traveled distance of the fingertip between contacts and thereby speed up the exploration. When evaluating an exploration strategy, the overall traveled distance of the exploring end-effector can be used as exploration cost and serve as evaluation metric for the exploration strategy in question.

We propose a novel next best touch target selection strategy based on the concept of information gain maximization that takes into account the minimization of exploration cost.

2.1. *Exploration algorithm*

During exploration of unknown objects, two connected problems have to be solved: the generation of exploratory actions to acquire contact data and the estimation of the object surface based on the sparse tactile data. Based on this surface estimation, the next exploratory action can be planned and executed. In this work, we focus on the exploration of an unknown object using one finger equipped with a sensor that yields contact information as well as surface orientation at the contact point. To start the exploration process, the algorithm is initialized with an initial target position within the object and the start position of the fingertip.

To establish initial contact with the object, the fingertip follows a direct approach to the initial touch target. When the fingertip is in contact with the object the contact position c_p and contact normal c_n are measured. Using this information, the initial model of the object is estimated.

The estimated surface is triangulated using Marching Cubes[35] near the latest contact point. For each triangle the central point is calculated along with its

Table 1. Summary of used symbols.

Function/symbol	Description
$\boldsymbol{r}, \boldsymbol{v}, \boldsymbol{\omega} \in \mathbb{R}^3$	End-effector position, linear velocity and angular velocity
$\boldsymbol{R} \in \mathrm{SO}(3)$	End-effector orientation
$T_p(\tau) : \mathbb{R} \to \mathbb{R}^3$	Trajectory position function
$T_R(\tau) : \mathbb{R} \to \mathrm{SO}(3)$	Trajectory orientation function
$\tau \in [0, 1]$	Argument of the trajectory function $T(\tau = 0)$: trajectory start, $T(\tau = 1)$: trajectory end
$\mathcal{C}$	Set of all contacts
$\boldsymbol{c}_p, \boldsymbol{c}_n \in \mathbb{R}^3$	Position and normal of a contact in $\mathcal{C}$
$\mathcal{S}$	Surface estimation
$\boldsymbol{s}_p, \boldsymbol{s}_n \in \mathbb{R}^3$	Position and normal of a point on $\mathcal{S}$
$\boldsymbol{t}_p, \boldsymbol{t}_n \in \mathbb{R}^3$	Position and normal of the selected target on $\mathcal{S}$
$\Delta m \in \mathbb{R}$	Distance that defines when a target is considered missed
$\sigma_1, \sigma_3, \mu_3, \sigma_\alpha \in \mathbb{R}$	Tuning parameters
$v_0 \in \mathbb{R}$	Desired velocity of the end-effector

corresponding normal. For each point the estimated information gain is evaluated by either employing the state-of-the-art GP-V or the IGEF proposed in this work.

2.2. *Selection of the next best touch target*

In order to perform an efficient exploration of an unknown object, each new contact should result in new information. Additionally, the cost to acquire the next contact, i.e., the distance between the previous and the next contact, should be minimized. We define the information gained (Δ information) by the amount of surface on the object that is newly explored by the touch. The cost (Δ cost) of one exploratory action is defined by the length of the path between the new contact and the last contact. A point on the actual object surface is considered explored if a previously explored contact point lies within a given radius r. The information gain Δ information is equivalent to the newly-explored part of the object that is added by a contact. The goal of an efficient exploration algorithm is to maximize the information gain per cost:

$$\text{Maximize} \frac{\Delta \text{ information}}{\Delta \text{ cost}}. \tag{1}$$

Maximizing the fraction in Eq. (1) can be achieved by maximizing the amount of information gained by each exploratory action and by minimizing the cost per exploratory action.

2.3. *Gaussian variance-based exploration*

GPIS are widely used to estimate the surface of an unknown object based on haptic contact data.[18–22] Thereby, the GPIS potential function $f(x) : \mathbb{R}^3 \to \mathbb{R}$ is given by

$$f(x) = k_*(x)^T (K + \sigma^2 I)^{-1} y, \tag{2}$$

Algorithm 1 Algorithm of the proposed haptic exploration strategy

$\boldsymbol{r} \leftarrow$ *start position*
$\boldsymbol{t}_p \leftarrow$ *initial target*
$\boldsymbol{v}_n \leftarrow (\boldsymbol{t}_p - \boldsymbol{r})\|\boldsymbol{t}_p - \boldsymbol{r}\|^{-1}$ ▷ initial approach velocity
setVelocity($\boldsymbol{v}_n v_0$)
repeat
  waitUntilContact()
  $\boldsymbol{c}_p \leftarrow$ *contact position*
  $\boldsymbol{c}_n \leftarrow$ *contact normal*
  $\boldsymbol{v}_n \leftarrow$ *current normalized velocity*
  setVelocity($\boldsymbol{0}$) ▷ stop until new trajectory is calculated
  $\mathcal{C} \leftarrow \mathcal{C} \cup \{(\boldsymbol{c}_p, \boldsymbol{c}_n)\}$ ▷ add new contact to contact set
  $\mathcal{S} \leftarrow$ *GPIS*($\mathcal{C}$)
  if target strategy **is** GP variance **then**
    $\forall \boldsymbol{s} \in \mathcal{S} : I(\boldsymbol{s}) \leftarrow$ *GP variance*($\boldsymbol{s}$)
  if target strategy **is** Information Gain Estimation Function **then**
    $I(\mathcal{S}) \leftarrow$ *Information Gain Estimation Function*($\mathcal{S}$) ▷ see Algorithm 2
  $\boldsymbol{t} \leftarrow \text{argmax}_{\boldsymbol{s}}\, I(\boldsymbol{s})$
  $\boldsymbol{R}_0 \leftarrow$ *current orientation*
  $\boldsymbol{R}_1 \leftarrow \text{getRotation}(\boldsymbol{R}_0, \boldsymbol{t}_n)$
  $\beta \leftarrow \frac{1}{3}\|\boldsymbol{c}_p - \boldsymbol{t}_p\|$ ▷ control point scaling
  $T_p \leftarrow \text{bezier}(\boldsymbol{c}_p, \boldsymbol{c}_p - \beta\boldsymbol{v}_n, \boldsymbol{t}_p + \beta\boldsymbol{t}_n, \boldsymbol{t}_p)$ ▷ trajectory from $\boldsymbol{c}$ to $\boldsymbol{t}$
  $T_R \leftarrow \text{lerp}(\boldsymbol{R}_0, \boldsymbol{R}_1)$
  $\tau \leftarrow 0$
  repeat ▷ Cartesian velocity controller
    $\boldsymbol{r} \leftarrow$ *current position*
    $\boldsymbol{R} \leftarrow$ *current orientation*
    $\tau \leftarrow \text{argmin}_{\tau_\star \in [\tau, 1]}\|\boldsymbol{r} - T(\tau_\star)\|$ ▷ find closest point on trajectory
    if $\tau > 1$ **and** $\|\boldsymbol{r} - T(1)\| > \Delta m$ **then** ▷ missed prediction
      $\boldsymbol{v}_n \leftarrow$ *current normalized velocity*
      $\beta \leftarrow \frac{1}{3}\|\boldsymbol{r} - \boldsymbol{t}_p\|$ ▷ control point scaling
      $T_p \leftarrow \text{bezier}(\boldsymbol{r}, \boldsymbol{r} + \beta\boldsymbol{v}_n, \boldsymbol{t}_p - \beta\boldsymbol{t}_n, \boldsymbol{t}_p)$ ▷ trajectory from $\boldsymbol{r}$ to $\boldsymbol{t}$
      $\boldsymbol{R}_0 \leftarrow R$
      $\boldsymbol{R}_1 \leftarrow \text{getRotation}(\boldsymbol{R}_0, -\boldsymbol{t}_n)$ ▷ inverted target approach
      $T_R \leftarrow \text{lerp}(\boldsymbol{R}_0, \boldsymbol{R}_1)$
      $\tau \leftarrow 0$
    $v_* \leftarrow T_p(\tau + \Delta\tau) - \boldsymbol{r}$
    $v_n \leftarrow \boldsymbol{v}_*\|\boldsymbol{v}_*\|^{-1}$ ▷ normalize velocity
    setVelocity($\boldsymbol{v}_n v_0$)
    $\boldsymbol{\omega} \leftarrow \text{rollPitchYaw}(\boldsymbol{R}^{-1} T_R(\tau))$ ▷ get angular velocity
    setAngularVelocity($\boldsymbol{\omega}$)
  until contact
until object explored

where K is the covariance matrix, which is computed by evaluating the kernel function between all combinations of observed sample locations x_i, x_j:

$$K_{i,j} = k(x_i, x_j). \tag{3}$$

The covariance vector between a query point x and the observed samples x_i is given by

$$k_{*,i}(x) = k(x, x_i). \tag{4}$$

A common choice for the kernel function k is the Gaussian kernel

$$k(x_i, x_j) = \exp\left(-\frac{\|x_i - x_j\|^2}{\sigma^2}\right). \tag{5}$$

Besides the implicit shape potential (ISP), Gaussian processes also yield a variance Q. State-of-the-art approaches suggest to use this variance of Gaussian processes to select the next best target for exploration.[19,22] The variance is defined by

$$Q(x) = k(x, x) - k_*^T (K + \sigma^2 I)^{-1} k_*. \tag{6}$$

When using the Gaussian kernel function the variance Q is bounded to $[0, 1]$. The variance Q is close to 0 when evaluated next to an observed sample point x_i whereas Q gets close to 1 when evaluated far away from any observed sample x_i. Thus, using the Gaussian variance for exploration leads to a maximization of the newly-gained information Δ information per exploratory action. The exploration always tries to gain as much new information as possible, without considering the cost of the next action. This is a valid approach and has been used in the state-of-the-art, resulting in a successful exploration of an unknown object.[19,22] However, the targets selected by this approach tend to be very far apart, leading to a large cost in terms of traveled distance during the exploratory actions.[21]

2.4. *Information gain estimation function*

In order to gain new information about the unknown object as fast as possible we combine the goal of maximizing the newly gained information with the minimization of the expected cost for each action. Similarly to Gaussian variance-based approaches, we employ Gaussian kernels to estimate the gained information. We distinguish between four different goals that should be considered during exploration:

(1) *Uncertainty*: Each exploratory action should yield the maximum amount of new information.
(2) *Cost*: The cost of each exploratory action should be minimized.
(3) *Locality*: Prefer targets that are close to already-explored regions.
(4) *Rotation*: Minimize the rotation of the fingertip during an exploratory action.

The first goal is implemented as a greedy metric that tries to gain the maximum new information per contact possible. The other three goals are designed to counterbalance this greediness and produce exploration actions suited for local exploration.

Each goal is characterized by a metric $(\Psi_1 \cdots \Psi_4)$. The *first metric* Ψ_1 tries to maximize the gained information by penalizing targets that are close to already-explored contacts. In fact, Ψ_1 is zero when evaluated directly at a previously observed contact point c_i. This metric drives the exploration to previously-unexplored regions of the object. Adding contacts in new regions reduces the uncertainty of the estimated surface:

$$\Psi_1(\boldsymbol{s}_p, \boldsymbol{c}_p) := 1 - \exp\left(-\frac{\|\boldsymbol{s}_p - \boldsymbol{c}_p\|^2}{{\sigma_1}^2}\right). \tag{7}$$

The *second metric* Ψ_2 follows our definition of the cost function by directly measuring the length of the planned path from the current position $\boldsymbol{r}$ to the target touch point $\boldsymbol{s}$. This metric serves multiple purposes. Most importantly it leads to local exploration where the estimated surface is not likely to diverge greatly from the actual object. Secondly, it reduces to time spent moving the end-effector from contact-to-contact

$$\Psi_2(\boldsymbol{s}) := \frac{1}{\mathrm{Len}(\mathrm{path}(\boldsymbol{r}, \boldsymbol{s}))}, \tag{8}$$

where the length of the path is calculated as the arc length of the curve

$$\mathrm{Len}(T(\tau)) = \int_0^1 \left\| \frac{\partial T}{\partial \tau} \right\| d\tau. \tag{9}$$

The *third metric* Ψ_3 prefers targets that are close to already-explored regions. The next point should be at a distance approximately μ_3 to any of the previous contacts points. This metric encourages an exploration scheme that follows roughly a spiral, as can be seen in Fig. 2. If Ψ_3 is omitted the exploration sometimes just follows a straight line, not exploring the local surroundings. To achieve this, we use a Gaussian distribution with offset mean μ_3:

$$\Psi_3(\boldsymbol{s}, \boldsymbol{c}) := \exp\left(-\frac{(\|\boldsymbol{s} - \boldsymbol{c}\| - \mu_3)^2}{{\sigma_3}^2}\right). \tag{10}$$

The *fourth metric* Ψ_4 is an angular kernel, measuring the distance between the current orientation of the fingertip and the estimated surface normal at the touch target s_n as proposed in[36]:

$$\Psi_4(\boldsymbol{s}) := \exp\left(-\frac{2\sin^2\left(\frac{1}{2}\arccos(R_z, \boldsymbol{s}_n)\right)}{{\sigma_\alpha}^2}\right). \tag{11}$$

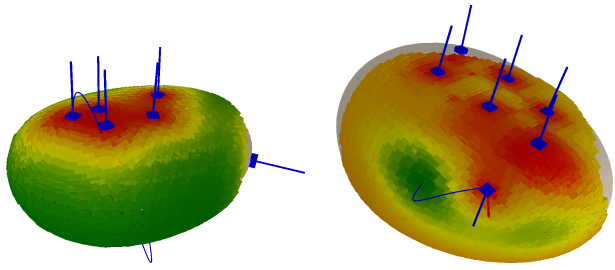

(a) (b)

Fig. 1. State-of-the-art Gaussian variance-based exploration approaches lead to greedy target selection without path cost consideration (a). The proposed IGEF prefers local targets while minimizing path cost (b). Already-acquired contacts with respective normals are shown in blue. The coloring of the estimated surface indicates the expected information gain, where red areas have no predicted information gain and green areas have the highest predicted information gain.

These four metrics have been designed to be combined by multiplication to describe the overall exploration metric Ψ:

$$\Psi = \prod_{n=1}^{4} \Psi_n. \tag{12}$$

For the evaluation on the YCB object set, the parameters σ_1, μ_3 and σ_3 have all been set to 2 cm while σ_α has been set to 1.

The estimated surface $\mathcal{S}$ is sampled, starting from the last contact position. The sample step length was set to 0.5 cm with a maximum radius of 5 cm. The next best touch target is selected by choosing the sample point that maximizes the IGEF. An example of the sampling is depicted in Fig. 1.

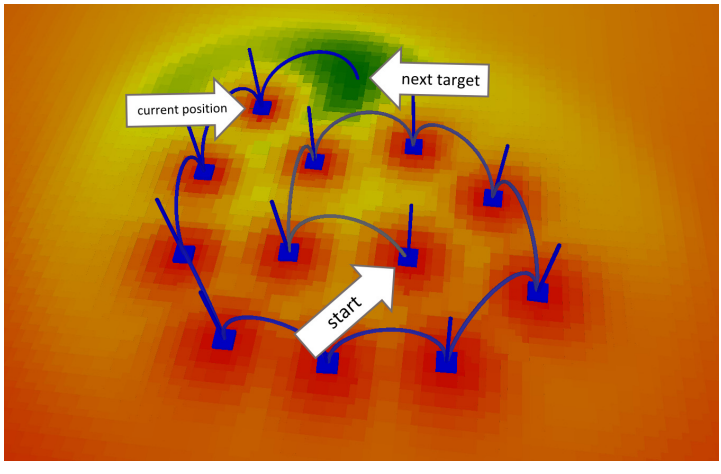

Fig. 2. Exemplary exploration of a flat plane. The combination of the exploration goals Ψ_1, Ψ_2 and Ψ_3 leads to an exploratory path that roughly follows an outward spiral. In green areas the predicted information gain is high, in red areas it is low.

Algorithm 2 Calculation of the information gain estimation function metrics

Input $S, \mathcal{C}, r, v_n$
for $s \in S$ **do**
  $\Psi_1(\boldsymbol{s}) \leftarrow \min_{\boldsymbol{c}} \Psi_1(\boldsymbol{s}, \boldsymbol{c})$ ▷ see Eq. (7)
  $\Psi_2(\boldsymbol{s}) \leftarrow \mathrm{Len}(\mathrm{bezier}(\boldsymbol{r}, \boldsymbol{r} - \boldsymbol{v}_n\|\boldsymbol{r} - \boldsymbol{s}_p\|, \boldsymbol{s}_p + \boldsymbol{s}_n\|\boldsymbol{r} - \boldsymbol{s}_p\|, \boldsymbol{s}_p))^{-1}$ ▷ see Eq. (8)
  $\Psi_3(\boldsymbol{s}) \leftarrow \sum_{\boldsymbol{c}} \Psi_3(\boldsymbol{s}, \boldsymbol{c})$ ▷ see Eq. (10)
  $\Psi_4(\boldsymbol{s}) \leftarrow 1 - \exp\left(-2\sin^2\left(\frac{1}{2}\alpha(R_z, \boldsymbol{s}_n)\right)\sigma_\alpha^{-2}\right)$ ▷ see Eq. (11)
return $\Psi_1\Psi_2\Psi_3\Psi_4$ ▷ see Eq. (12)

2.5. *Trajectory generation*

The trajectory $T(\tau)$ for the fingertip has to be generated to reach the selected touch target. This trajectory has to start at the current position $\boldsymbol{r}$ and to end at the target $\boldsymbol{t}_p$ while following a continuous path. For this purpose, we use cubic bezier curves which are defined by four points: the start point $\boldsymbol{p}_0$, the target touch point $\boldsymbol{p}_3$, and two control points $\boldsymbol{p}_1$ and $\boldsymbol{p}_2$ describing the shape of the curve. In addition, the target should be approached parallel to the estimated surface normal direction $\boldsymbol{t}_n$ at the target.

The Cartesian velocity vector just before contact is stored in $\boldsymbol{v}_n$. The retraction movement of the fingertip is performed alongside $-\boldsymbol{v}_n$:

$$T(\tau) = \mathrm{bezier}(\boldsymbol{p}_0, \boldsymbol{p}_1, \boldsymbol{p}_2, \boldsymbol{p}_3), \tag{13}$$

$$\begin{pmatrix} T(0) \\ T(1) \\ \dfrac{\partial T(0)}{\partial \tau} \\ \dfrac{\partial T(1)}{\partial \tau} \end{pmatrix} = \begin{pmatrix} \boldsymbol{p}_0 \\ \boldsymbol{p}_3 \\ 3(\boldsymbol{p}_1 - \boldsymbol{p}_0) \\ 3(\boldsymbol{p}_2 - \boldsymbol{p}_3) \end{pmatrix} = \begin{pmatrix} \boldsymbol{r} \\ \boldsymbol{t}_p \\ -\boldsymbol{v}_n\|\boldsymbol{r} - \boldsymbol{t}_p\| \\ \boldsymbol{t}_n\|\boldsymbol{r} - \boldsymbol{t}_p\| \end{pmatrix}, \tag{14}$$

$$T(\tau) = \mathrm{bezier}\left(\boldsymbol{r}, \boldsymbol{r} - \frac{1}{3}\boldsymbol{v}_n\|\boldsymbol{r} - \boldsymbol{t}_p\|, \boldsymbol{t}_p + \frac{1}{3}\boldsymbol{t}_n\|\boldsymbol{r} - \boldsymbol{t}_p\|, \boldsymbol{t}_p\right). \tag{15}$$

The first control point is chosen to guide the retraction of the fingertip from the object surface. To this end, the first control point p_1 is defined by the negative approach velocity, which is scaled by the distance between the start and the target point. The second control point p_2 is chosen to lie on the normal of the estimated surface at the target point. Following this trajectory ensures that the velocity during exploration is continuous, thus the fingertip does not perform any high jerk motions.

The orientation of the fingertip is calculated by a linear interpolation between the start and the target orientation. The target orientation is calculated so that the fingertip is aligned with the surface normal at the target. Once a contact between the fingertip and the object surface is detected while following the trajectory the new

contact is added to the set of contact points and the surface estimation is updated using GPIS. If the trajectory is completed without any contact event, the estimation of the surface was incorrect. In this case, a new trajectory has to be generated that guides the fingertip back to the object surface:

$$\begin{pmatrix} T(0) \\ T(1) \\ \dfrac{\partial T(0)}{\partial \tau} \\ \dfrac{\partial T(1)}{\partial \tau} \end{pmatrix} = \begin{pmatrix} \boldsymbol{r} \\ \boldsymbol{t}_p \\ \boldsymbol{v}_n \|\boldsymbol{r} - \boldsymbol{t}_p\| \\ -\boldsymbol{t}_n \|\boldsymbol{r} - \boldsymbol{t}_p\| \end{pmatrix}, \tag{16}$$

$$T(\tau) = \text{bezier}\left(\boldsymbol{r}, \boldsymbol{r} + \frac{1}{3}\boldsymbol{v}_n\|\boldsymbol{r} - \boldsymbol{t}_p\|, \boldsymbol{t}_p - \frac{1}{3}\boldsymbol{t}_n\|\boldsymbol{r} - \boldsymbol{t}_p\|, \boldsymbol{t}_p\right). \tag{17}$$

The requirements from Eq. (16) lead to the parametrization of the cubic bezier in Eq. (17). Note that the signs of the parameters defining the control points are flipped compared to the signs in Eq. (15). This ensures that the velocity is continuous when the actual surface of the object is missed. This also ensures that contact with the object is always re-established, since the target position is the last contact point. Figure 3 shows an example of such a situation.

2.6. *Comparison*

In this section, the approach based on the GP-V and the proposed IGEF are illustrated using example situations that arise during exploration. Figure 4 shows the resulting target ratings after the second contact for GP-V and IGEF, respectively. The blue curve indicates the trajectory to the planned third target. The maximum

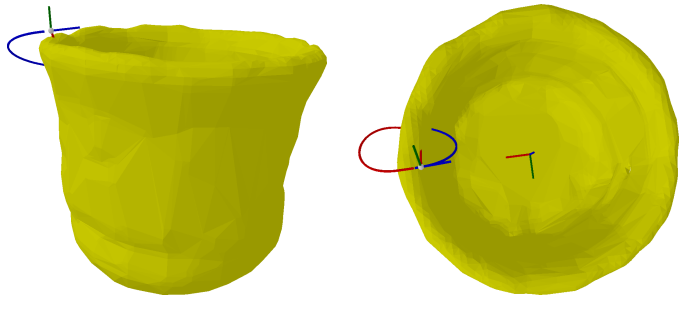

(a) (b)

Fig. 3. Example trajectory of a missed edge. The predicted surface contact does not lie on the actual object surface and thus the calculated trajectory misses the object (a). The trajectory is continued to re-establish contact with the object by approaching the previous contact (b).

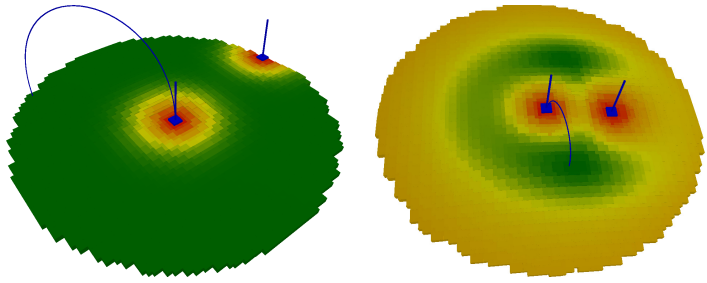

(a) GP-V (b) IGEF

Fig. 4. Predicted information gain after the second contact on a flat surface. The GP-V approach suggests a target that lies on the edge of the allowed area (a). The IGEF-based strategy prefers a target that is closer to the existing contacts to minimize path cost (b). The trajectory to the next best touch target is depicted as a blue curve.

allowed target distance has to be limited in practice, otherwise the GP-V approach tends to suggest targets that are very far away, leading to an infeasible exploratory action. The target suggested by GP-V lies at the border of the allowed target distance (in our experiments we chose 6 cm).

Figure 1 depicts the predicted information gain after several contacts with the object have been established. It can be seen that the greedy nature of the GP-V approach suggests a target on the back side of the estimated surface. In contrast, the IGEF approach suggests a closer target leading to a shorter exploration trajectory. The scatterplots in Fig. 5 correspond to the states depicted in Fig. 1. The main difference is that the IGEF approach has a clear maximum at a distance of 2.1 cm whereas GP-V is not as decisive and rates many targets close to the maximum of 1.

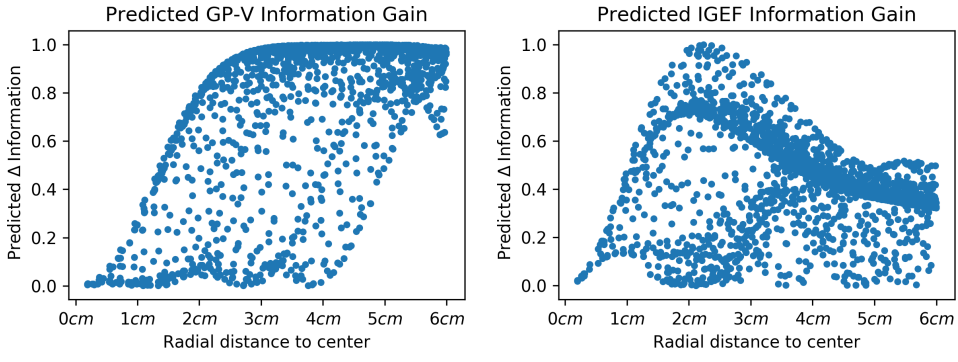

(a) (b)

Fig. 5. Predicted information gain after several contacts. The GP-V approach rates multiple targets close to the maximum rating of 1 (a) while IGEF suggests a maximum rating of 1 only in a small region (b).

3. Evaluation

The evaluation of the presented IGEF exploration strategy is performed in simulation. We use a subset of 48 objects from the YCB Object and Model Set.[34] The remaining object meshes were less-suited for exploration due to imprecisions in the meshes. The objects used in this work are listed together with the achieved results in Table 4.

3.1. *Exemplary evaluation run*

To illustrate the exploration procedure, Fig. 6 depicts the trajectory of the fingertip during the exploration of the banana from the YCB Object and Model Set.

The greedy behavior of the GP-V approach leads to a wide distribution of contact points, resulting in a longer trajectory of the fingertip. This can also be seen in Fig. 7, where the overall estimated surface RMSE drops quickly while the explored fraction of the ground truth mesh increases slowly at the end. The IGEF strategy however tends to explore more locally, leading to a shorter trajectory per acquired contact.

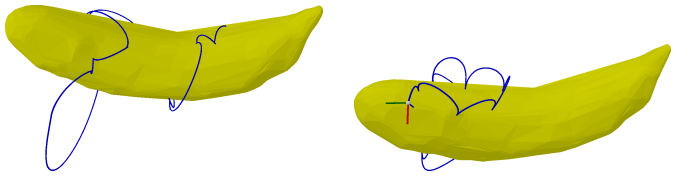

(a) GP-V (b) IGEF

Fig. 6. Exemplary exploration progress of the YCB banana. The blue line depicts the complete trajectory during the exploration. Following the GP-V leads to long jumps across the surface resulting in a high travel cost (a). The targets generated by the IGEF approach lie closer together forming a dense pattern with short hops between contact points (b).

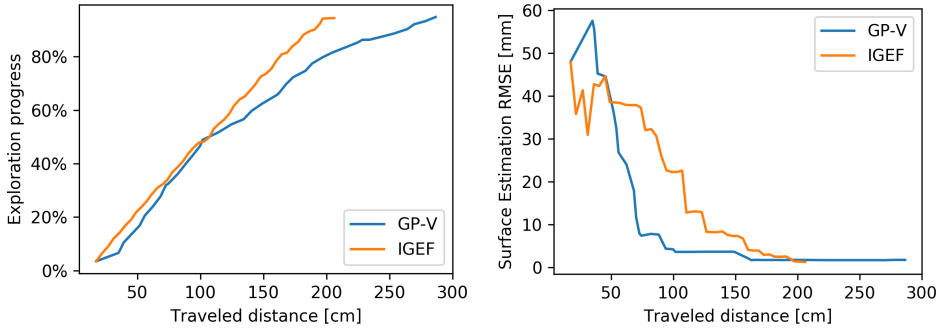

(a) Exploration progress (b) Estimated surface RMSE

Fig. 7. Exemplary exploration progress of the YCB banana.

The trajectory consists of many small local hops. This leads to a steady increase of explored portion over traveled fingertip distance. However, the overall RMSE drops more slowly when compared to GP-V, while eventually reaching the same final quality. Another exemplary run is depicted in Fig. 8, leading to a complete reconstruction of the object.

3.2. *Evaluation procedure*

The exploration algorithm is run 10 times for each of the 48 objects. Each evaluation run is started with different initial conditions: the start position of the end-effector is changed so that the initial approach direction to the objects is varied. This induces some initial variance into the exploration so that the initial contact occurs at varying locations on the object's surface.

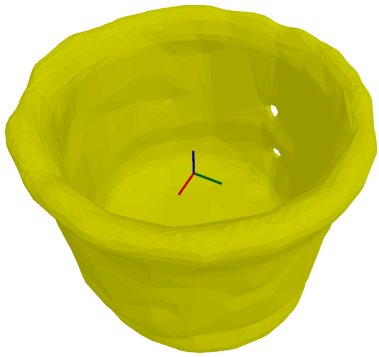

(a) Ground truth mesh

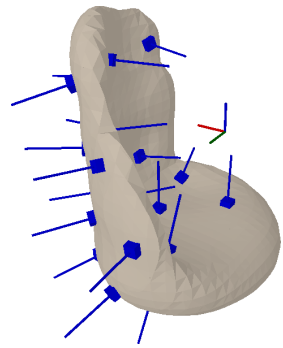

(b) Intermediate result based on 27-oriented contacts

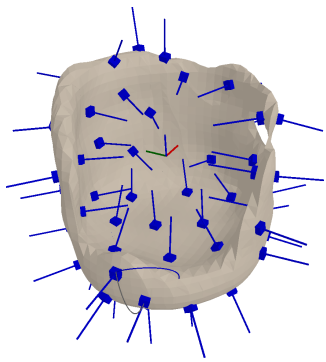

(c) Intermediate result based on 73-oriented contacts

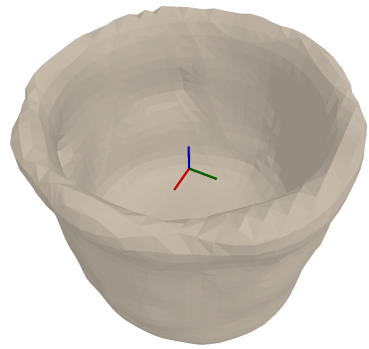

(d) Final reconstruction based on 117-oriented contacts

Fig. 8. The IGEF-based approach leads to a complete and cost-aware exploration of an unknown object (YCB object No. 25).

All values we provide are averages over the 10 evaluation runs. For each contact, an area of 6 mm around it is marked as explored on the ground truth mesh. One evaluation run is considered completed when at least 80% of the ground truth mesh is marked explored. Sometimes a small part of the object could not be covered by the exploration, because it was not reachable. Therefore, we decided to use 80% exploration coverage instead of 100%. We also compared the results when the exploration reached 50% coverage.

In our evaluation, we consider the following four metrics:

(1) *Traveled distance*: The overall path length of all exploratory actions until the object is explored.
(2) *Overall rotation*: The accumulated rotation of the fingertip orientation during all exploratory actions.
(3) *Surface RMSE*: The root-mean-square-error (RMSE) between the ground truth mesh and the triangulated estimated surface after the exploration has finished.
(4) *Prediction miss*: The average distance between the predicted contact based on the estimated surface and the actual contact with the ground truth mesh.

Table 2. Results for YCB object dataset.

Coverage (%)	Metric	GP-V	IGEF	Avg. Improvement (%)
50	Avg. traveled distance	103 cm	78 cm	22
	Avg. overall rotation	560°	474°	15
	Avg. surface RMSE	1.32 mm	1.04 mm	20
	Avg. prediction miss	25 mm	7 mm	72
	Avg. number of contacts	12.0	15.0	—
80	Avg. traveled distance	159 cm	117 cm	26
	Avg. overall rotation	995°	803°	19
	Avg. surface RMSE	1.01 mm	0.89 mm	11
	Avg. prediction miss	17 mm	5 mm	67
	Avg. number of contacts	19.4	24.3	—

Table 3. Results for YCB object dataset using LIS for exploration.

Coverage (%)	Metric	GP-V	IGEF	Avg. Improvement (%)
50	Avg. traveled distance	160 cm	90 cm	44
	Avg. overall rotation	754°	617°	10
	Avg. surface RMSE	1.56 mm	1.3 mm	19
	Avg. prediction miss	39 mm	10 mm	75
	Avg. number of contacts	9.9	15.6	—
80	Avg. traveled distance	289 cm	132 cm	54
	Avg. overall rotation	1393°	913°	34
	Avg. surface RMSE	1.09 mm	0.88 mm	19
	Avg. prediction miss	37 mm	9 mm	75
	Avg. number of contacts	19.2	24.5	—

Table 4. Results for YCB object dataset.

No.	Object name	GP-V (cm)	IGEF (cm)	Improvement (%)
1	block_of_wood_6in	262.6	216.7	17.5
2	blue_wood_block_1inx1in	45.7	33.5	26.7
3	brine_mini_soccer_ball	435.5	221.0	49.3
4	campbells_condensed_tomato_soup	203.5	170.9	16.0
5	champion_sports_official_softball	236.8	197.3	16.7
6	dark_red_foam_block_with_three_holes	152.1	116.4	23.4
7	expo_black_dry_erase_marker	82.0	70.5	14.0
8	frenchs_classic_yellow_mustard_14oz	258.8	221.1	14.6
9	jell-o_chocolate_flavor_pudding	219.5	173.3	21.0
10	jell-o_strawberry_gelatin_dessert	146.7	110.3	24.8
11	master_chef_ground_coffee_297g	427.2	217.3	49.1
12	medium_black_spring_clamp	112.8	93.7	16.9
13	melissa_doug_farm_fresh_fruit_apple	162.0	132.3	18.3
14	melissa_doug_farm_fresh_fruit_banana	167.6	181.3	−8.2
15	melissa_doug_farm_fresh_fruit_lemon	87.4	71.7	18.0
16	melissa_doug_farm_fresh_fruit_orange	136.3	114.2	16.2
17	melissa_doug_farm_fresh_fruit_peach	114.8	95.3	17.0
18	melissa_doug_farm_fresh_fruit_pear	134.6	110.0	18.3
19	melissa_doug_farm_fresh_fruit_plum	77.8	64.7	16.8
20	melissa_doug_farm_fresh_fruit_strawberry	59.6	49.0	17.7
21	morton_salt_shaker	99.3	92.8	6.6
22	moutain_security_steel_shackle	54.3	48.2	11.1
23	orange_wood_block_1inx1in	46.8	35.4	24.4
24	penn_raquet_ball	79.3	67.1	15.5
25	play_go_rainbow_stakin_cups_10_blue	388.9	229.8	40.9
26	play_go_rainbow_stakin_cups_1_yellow	88.9	71.9	19.1
27	play_go_rainbow_stakin_cups_2_orange	91.0	76.6	15.9
28	play_go_rainbow_stakin_cups_3_red	107.3	85.6	20.2
29	play_go_rainbow_stakin_cups_5_green	143.6	112.9	21.3
30	play_go_rainbow_stakin_cups_6_purple	222.4	161.9	27.2
31	play_go_rainbow_stakin_cups_7_yellow	182.0	143.5	21.2
32	play_go_rainbow_stakin_cups_8_orange	301.2	211.6	29.7
33	play_go_rainbow_stakin_cups_9_red	340.8	221.6	35.0
34	play_go_rainbow_stakin_cups_blue_4	118.9	99.0	16.7
35	purple_wood_block_1inx1in	45.7	36.1	21.0
36	red_metal_cup_white_speckles	373.8	209.2	44.0
37	red_wood_block_1inx1in	45.5	35.0	23.0
38	sharpie_marker	61.6	55.8	9.5
39	small_black_spring_clamp	84.6	75.2	11.2
40	spam_12oz	217.1	184.7	14.9
41	sponge_with_textured_cover	121.1	125.3	−3.5
42	stainless_steel_fork_red_handle	62.6	51.5	17.8
43	stanley_flathead_screwdriver	68.4	59.6	12.8
44	stanley_philips_screwdriver	69.5	58.0	16.6
45	starkist_chunk_light_tuna	150.6	120.2	20.2
46	thick_wood_block_6in	476.6	214.2	55.0
47	wilson_golf_ball	54.3	44.9	17.2
48	yellow_wood_block_1inx1in	45.3	36.0	20.5
	Average	159.7	117.2	20.6

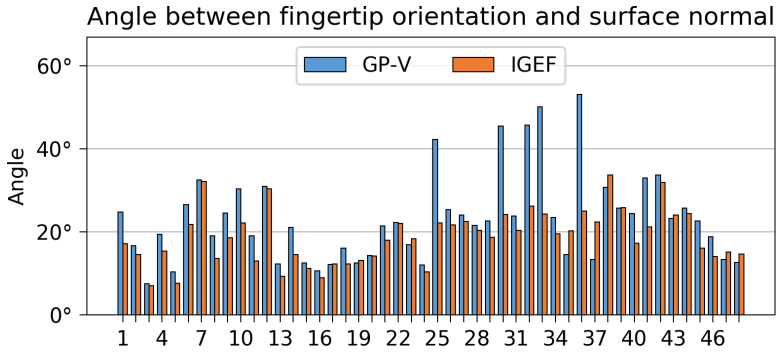

Fig. 9. Angle between the fingertip orientation and the actual surface normal during contact.

We use Gaussian Process Implicit Surfaces with a thin-plate kernel for surface modeling.[17] The average results of all evaluation runs can be found in Table 2. On average, the IGEF-based exploration outperforms the GP-V-based exploration. For most objects the proposed IGEF strategy performs better than GP-V approach, although there are some objects for which GP-V performs slightly better (object 14 and 41).

To show that the IGEF approach works independently of the chosen surface estimation model, we repeated the complete evaluation with our previously-proposed Local Implicit Surface (LIS) approach.[37] This approach is designed to reproduce edges and corners more accurately than GPIS. In some cases the estimated surface of LIS differs notably from the GPIS estimation. However, applying the IGEF strategy still produces improved results when compared to the GP-V baseline. The average results can be found in Table 3.

Another important aspect for exploration is the angle between the fingertip and the actual surface normal during contact, since many real haptic sensors have a limited measurable angle between sensor orientation and surface normal. For example the IMU-based surface orientation sensor proposed by Kaul *et al.* works best for approach directions within a 30° cone around the surface normal.[38] Similarly, Zhe *et al.* reported feasibility of the BioTac Sensor for surface orientation measurement in the range of ±7° for pitch and roll.[39] For each object in the test set the average angle between surface normal and fingertip orientation during contact is depicted in Fig. 9. For most objects the IGEF approach performs better (i.e., produces a smaller angle) on average when compared to GP-V-based exploration.

4. Conclusion and Future Work

In this work, we presented a novel haptic exploration strategy for unknown objects based on local information maximization and exploration cost minimization. We conducted an extensive evaluation in simulation using 48 objects from the YCB object and model set and we showed that the proposed IGEF outperforms

GP-V-based methods for touch target selection. The evaluation results are based on four metrics considering the overall path length of all exploratory motions, the overall rotation of the fingertip during exploration, the average distance between predicted contact and actual contact with the ground truth object as well as the surface reconstruction quality measured by RMSE between the estimated surface and the ground truth mesh. The proposed approach depends on several tuning parameters that have been manually chosen for best performance. Tuning these parameters could be automated in the future, e.g., by machine learning approaches. Furthermore, we intend to validate the proposed approach on the humanoid robot ARMAR-III[40] with a tactile sensor providing contact data and surface orientation as described in our previous work.[38]

Acknowledgments

The research leading to these results has received funding from the European Unions Horizon 2020 Research and Innovation programme under Grant Agreement No. 643950 (SecondHands) and from the German Research Foundation (DFG) under the Priority Program on Autonomous Learning (SPP 1527).

References

1. R. S. Johansson and J. R. Flanagan, Coding and use of tactile signals from the fingertips in object manipulation tasks, *Nat. Rev. Neurosci.* **10**(5) (2009) 345–359.
2. H. Gu, Y. Zhang, S. Fan, M. Jin and H. Liu, Grasp configurations optimization of dexterous robotic hand based on haptic exploration information, *Int. J. Hum. Robot.* **14**(4) (2017) 1750013.
3. M. Kaboli, D. Feng and G. Cheng, Active tactile transfer learning for object discrimination in an unstructured environment using multimodal robotic skin, *Int. J. Hum. Robot.* **1** (2018) 1850001.
4. Y. Kuniyoshi, R. Fukano, T. Otani, T. Kobayashi and N. Otsu, Haptic detection of object affordances by a multi-fingered robot hand, *Int. J. Hum. Robot.* **2**(4) (2005) 415–435.
5. A. Bierbaum, M. Rambow, T. Asfour and R. Dillmann, Grasp affordances from multi-fingered tactile exploration using dynamic potential fields, in *IEEE–RAS Int. Conf. Humanoid Robots* (*Humanoids*) (Paris, France, 2009), pp. 168–174.
6. A. Petrovskaya and O. Khatib, Global localization of objects via touch, *IEEE Trans. Robotics* **27**(3) (2011) 569–585.
7. A. Bierbaum, M. Rambow, T. Asfour and R. Dillmann, A potential field approach to dexterous tactile exploration of unknown objects, in *IEEE–RAS Int. Conf. Humanoid Robots* (*Humanoids*) (IEEE 2008), pp. 360–366.
8. K. Duncan, S. Sarkar, R. Alqasemi and R. Dubey, Multi-scale superquadric fitting for efficient shape and pose recovery of unknown objects, in *IEEE Int. Conf. Robotics and Automation* (*ICRA*) (IEEE 2013), pp. 4238–4243.
9. A. Leonardis, A. Jaklic and F. Solina, Superquadrics for segmenting and modeling range data, *IEEE Trans. Pattern Anal. Mach. Intell.* **19**(11) (1997) 1289–1295.
10. H. Zha, T. Hoshide and T. Hasegawa, A recursive fitting-and-splitting algorithm for 3D object modeling using superquadrics, in *Int. Conf. Pattern Recognition*, Vol. 1 (IEEE 1998), pp. 658–662.

11. Z.-C. Marton, L. Goron, R. B. Rusu and M. Beetz, Reconstruction and verification of 3D object models for grasping, in *Robotics Research* (Springer, New York, 2011), pp. 315–328.
12. K. Huebner, S. Ruthotto and D. Kragic, Minimum volume bounding box decomposition for shape approximation in robot grasping, in *IEEE Int. Conf. Robotics and Automation* (*ICRA*) (IEEE 2008), pp. 1628–1633.
13. D. Schiebener, A. Schmidt, N. Vahrenkamp and T. Asfour, Heuristic 3D object shape completion based on symmetry and scene context, in *IEEE/RSJ Int. Conf. Intelligent Robots and Systems* (*IROS*) (IEEE 2016), pp. 74–81.
14. S. Thrun and B. Wegbreit, Shape from symmetry, in *IEEE Int. Conf. on Computer Vision*, Vol. 2 (IEEE 2005), pp. 1824–1831.
15. A. H. Quispe, B. Milville, M. A. Gutiérrez, C. Erdogan, M. Stilman, H. Christensen and H. B. Amor, Exploiting symmetries and extrusions for grasping household objects, in *IEEE Int. Conf. Robotics and Automation* (*ICRA*) (IEEE 2015), pp. 3702–3708.
16. J. Bohg, M. Johnson-Roberson, B. León, J. Felip, X. Gratal, N. Bergstrom, D. Kragic and A. Morales, Mind the gap — Robotic grasping under incomplete observation, in *IEEE Int. Conf. Robotics and Automation* (*ICRA*) (2011), pp. 686–693.
17. O. Williams and A. Fitzgibbon, Gaussian process implicit surfaces, in *Proc. of Gaussian Processes in Practice Workshop* (Bletchley, UK, June 2007).
18. S. Dragiev, M. Toussaint and M. Gienger, Gaussian process implicit surfaces for shape estimation and grasping, in *IEEE Int. Conf. Robotics and Automation* (*ICRA*) (IEEE 2011), pp. 2845–2850.
19. M. Bjorkman, Y. Bekiroglu, V. Hogman and D. Kragic, Enhancing visual perception of shape through tactile glances, in *IEEE/RSJ Int. Conf. Intelligent Robots and Systems* (*IROS*) (IEEE 2013), pp. 3180–3186.
20. N. Sommer, M. Li and A. Billard, Bimanual compliant tactile exploration for grasping unknown objects, in *IEEE Int. Conf. Robotics and Automation* (*ICRA*) (IEEE 2014), pp. 6400–6407.
21. T. Matsubara and K. Shibata, Active tactile exploration with uncertainty and travel cost for fast shape estimation of unknown objects, *Robot. Auton. Syst.* **91** (2017) 314–326.
22. Z. Yi, R. Calandra, F. Veiga, H. van Hoof, T. Hermans, Y. Zhang and J. Peters, Active tactile object exploration with Gaussian processes, in *IEEE/RSJ Int. Conf. Intelligent Robots and Systems* (*IROS*) (IEEE 2016), pp. 4925–4930.
23. W. Martens, Y. Poffet, P. R. Soria, R. Fitch and S. Sukkarieh, Geometric priors for Gaussian process implicit surfaces, *IEEE Robotics Automat. Lett.* **2**(2) (2017) 373–380.
24. H. Gu, Y. Zhang, S. Fan, M. Jin, H. Zong and H. Liu, Model recovery of unknown objects from discrete tactile points, in *IEEE Int. Conf. Advanced Intelligent Mechatronics* (*AIM*) (IEEE 2016), pp. 1121–1126.
25. H. Gu, S. Fan, H. Zong, M. Jin and H. Liu, Haptic perception of unknown object by robot hand: Exploration strategy and recognition approach, *Int. J. Hum. Robot.* **13**(3) (2016) 1650008.
26. P. Hebert, T. Howard, N. Hudson, J. Ma and J. W. Burdick, The next best touch for model-based localization, in *IEEE Int. Conf. Robotics and Automation* (*ICRA*) (IEEE 2013), pp. 99–106.
27. N. Jamali, C. Ciliberto, L. Rosasco and L. Natale, Active perception: Building objects' models using tactile exploration, in *IEEE–RAS Int. Conf. Humanoid Robots* (*Humanoids*) (IEEE 2016), pp. 179–185.
28. D. Tanaka, T. Matsubara, K. Ichien and K. Sugimoto, Object manifold learning with action features for active tactile object recognition, in *IEEE/RSJ Int. Conf. Intelligent Robots and Systems* (*IROS*) (IEEE 2014), pp. 608–614.

29. V. Ortenzi, H.-C. Lin, M. Azad, R. Stolkin, J. A. Kuo and M. Mistry, Kinematics-based estimation of contact constraints using only proprioception, in *IEEE–RAS Int. Conf. Humanoid Robots* (*Humanoids*) (IEEE 2016), pp. 1304–1311.
30. D. Driess, P. Englert and M. Toussaint, Active learning with query paths for tactile object shape exploration, in *2017 IEEE/RSJ Int. Conf. Intelligent Robots and Systems* (*IROS*) (2017), pp. 65–72.
31. S. Caselli, C. Magnanini, F. Zanichelli and E. Caraffi, Efficient exploration and recognition of convex objects based on haptic perception, in *IEEE Int. Conf. Robotics and Automation* (*ICRA*), Vol. 4 (IEEE 1996), pp. 3508–3513.
32. N. Tosi, O. David and H. Bruyninckx, Action selection for touch-based localisation trading-off information gain and execution time, in *IEEE Int. Conf. on Robotics and Automation* (*ICRA*) (IEEE 2014), pp. 2270–2275.
33. N. Sommer and A. Billard, Multi-contact haptic exploration and grasping with tactile sensors, *Robot. Auton. Syst.* **85** (2016) 48–61.
34. B. Calli, A. Singh, A. Walsman, S. Srinivasa, P. Abbeel and A. M. Dollar, The YCB object and model set: Towards common benchmarks for manipulation research, in *IEEE Int. Conf. Advanced Robotics* (*ICAR*) (IEEE 2015), pp. 510–517.
35. W. E. Lorensen and H. E. Cline, Marching cubes: A high resolution 3D surface construction algorithm, in *ACM Siggraph Computer Graphics*, Vol. 21 (ACM, 1987), pp. 163–169.
36. C. E. Rasmussen and C. K. Williams, *Gaussian Processes for Machine Learning*, Vol. 1 (MIT Press, Cambridge, 2006).
37. S. Ottenhaus, M. Miller, D. Schiebener, N. Vahrenkamp and T. Asfour, Local implicit surface estimation for haptic exploration, in *IEEE–RAS Int. Conf. Humanoid Robots* (*Humanoids*) (IEEE 2016), pp. 850–856.
38. L. Kaul, S. Ottenhaus, P. Weiner and T. Asfour, The sense of surface orientation in a new sensor modality for humanoid robots, in *IEEE–RAS Int. Conf. Humanoid Robots* (*Humanoids*) (IEEE 2016), pp. 820–825.
39. Z. Su, S. Schaal and G. E. Loeb, Surface tilt perception with a biomimetic tactile sensor, in *IEEE Int. Conf. Biomedical Robotics and Biomechatronics* (*BioRob*) (2016), pp. 936–943.
40. T. Asfour, K. Regenstein, P. Azad, J. Schroder, A. Bierbaum, N. Vahrenkamp and R. Dillmann, ARMAR-III: An integrated humanoid platform for sensory-motor control, in *IEEE–RAS Int. Conf. Humanoid Robots* (*Humanoids*) (IEEE 2006), pp. 169–175.

Simon Ottenhaus received his Diploma degree in Electrical Engineering from the University of Stuttgart, in 2014. He is currently a Ph.D. Student at the Institute for Anthropomatics and Robotics at KIT where he is a Member of the High-Performance Humanoid Technologies Lab. His major research interests are haptic exploration of unknown objects and modeling objects based on sparse data.

Lukas Kaul received his Master's degrees in Mechanical Engineering from the Karlsruhe Institute of Technology. He spent one semester at the Shanghai Jiao Tong University (China) and completed his Master's thesis work at the CSIRO Autonomous Systems Laboratory in Brisbane (Australia). He is currently a Ph.D. Student at the Institute for Anthropomatics and Robotics at KIT and a Member of the High-Performance Humanoid Technologies Lab.

His major research interests include novel sensor applications for humanoid robots as well as balancing and dynamic stabilization of bipedal robots.

Nikolaus Vahrenkamp received his Diploma and Ph.D. degrees from the Karlsruhe Institute of Technology (KIT), in 2005 and 2011, respectively. Currently, he is a Postdoctoral Researcher at the Institute for Anthropomatics and Robotics, High-Performance Humanoid Technologies Lab (H^2T). His research interests are motion planning, grasping and mobile manipulation, and software development for humanoid robots.

Tamim Asfour is Full Professor at the Institute for Anthropomatics and Robotics, Karlsruhe Institute of Technology (KIT) where he holds the Chair of Humanoid Robotics Systems and is Head of the High-Performance Humanoid Technologies Lab (H^2T). His current research interest is high performance 24/7 humanoid robotics. He is Developer and Leader of the development team of the ARMAR humanoid robot family. He has been active in the field of humanoid robotics for the last 17 years resulting in about 200 peer-reviewed publications with focus on engineering humanoids including humanoid mechatronics, grasping, dexterous and mobile manipulation, active perception, learning from human observation and experience as well as on the mechano-informatics of humanoids as the synergetic integration of mechatronics, informatics and artificial intelligence methods into integrated complete humanoid robot systems.